TÉCNICO LISBOA

Thesis Title

Ana Branca Medeiros Pais

Thesis to obtain the Master of Science Degree in

Mathematics and Applications

Supervisor(s): Doctor Cláudia Rita Ribeiro Coelho Nunes Philippart

Examination Committee

Chairperson: Prof. Full Name
Supervisor: Prof. Full Name 1 (or 2)
Member of the Committee: Prof. Full Name 3

Month 2018

Dedicated to someone special...

Acknowledgments

A few words about the university, financial support, research advisor, dissertation readers, faculty or other professors, lab mates, other friends and family...

Resumo

Inserir o resumo em Português aqui com o máximo de 250 palavras e acompanhado de 4 a 6 palavras-chave...

Palavras-chave: palavra-chave1, palavra-chave2,...

Abstract

Insert your abstract here with a maximum of 250 words, followed by 4 to 6 keywords...

Keywords: keyword1, keyword2,...

Contents

List of Tables

List of Figures

Chapter 1

Introduction

Insert your chapter material here...

1.1 Motivation

Relevance of the subject... Example Goals in the end of this mini chapter.

1.2 Optimal Stopping Problems

Definição.

Princípio de Programação Dinâmica.

HJB + Gerador infinitesimal de GBM

Investimento: região de continuação e de paragem

Outro tipo de problemas (para além dos de investimento)

Teorema da Verificação

1.3 Thesis Outline

O que se vai falar em cada capítulo. Referir que trabalhos extendemos ou se assemelham?

Chapter 2

Investing and entering the market with a new product

Insert your chapter material here...

2.1 Introduction

Situação do problema. Trabalhos já realizados e de maneira os extendemos.

Some overview of the underlying theory about the topic...

2.2 Stopping Problem

2.2.1 Benchmark Model

2.2.2 Capacity Optimization Model

2.3 Maximization Problem

Having calculated the expression of optimized value function F^*, our goal now is to calculate the optimal level of investment R, taking into account that it influences the waiting time for the breakthrough to happen. In order to do it, we need to maximize the expected value of the optimized value function.

Notice that the distribution of the waiting time is given by an Exponential with parameter $\lambda(R)$. Also, since we are interested to find the optimal level of investment made now, one may not forget to discount the optimized value function. Thus we obtain that our optimal level of investment leads to a value function given by

$$
\begin{aligned}
V(x) &= \max_R E\left[e^{-rt}F^*(x) - R\right] \\
&= \max_R \left\{ \int_0^\infty \lambda(R) e^{-\lambda(R)t} e^{-rt} F^*(x) dt - R \right\} \\
&= \max_R \left\{ \int_0^\infty \lambda(R) e^{-\lambda(R)t} e^{-rt} \sup_\tau E^{X_0=x}\left[\max_K e^{-r\tau} h(X_\tau, K) 1_{\{\tau<\infty\}}\right] dt - R \right\} \\
&= \max_R \left\{ \int_0^\infty \lambda(R) e^{-(\lambda(R)+r)t} \frac{(\theta x - \delta(r-\mu))^2}{4\alpha(r-\mu)x} - R \right\}
\end{aligned}
$$

Since $F^*(x)$ does not depend on investment R nor time t, and it only depends on the drift μ, the volatility σ of GBM, discount rate r, innovation level after the jump θ and sensibility parameters α and δ and noticing that $R^\gamma + r > 0$, since we have no negative investment, we obtain

$$
V(X) = \max_R \left\{ \frac{R^\gamma}{R^\gamma + r} F^*(x) - R \right\}.
$$

The optimal value of the investment to make, R^*, is found by analyzing the first and the second partial derivatives of the expression to maximize.

$$
\begin{aligned}
\frac{\partial}{\partial R}\left(\frac{R^\gamma}{R^\gamma + r} F^*(x) - R\right) &= \frac{\gamma R^{\gamma-1} F^*(x) r - (R^\gamma + r)^2}{(R^\gamma + r)^2} \\
\frac{\partial^2}{\partial R^2}\left(\frac{R^\gamma}{R^\gamma + r} F^*(x) - R\right) &= -\frac{F^*(x)\gamma r R^{-2+\gamma}(r - \gamma r + (1+\gamma)R^\gamma)}{(R^\gamma + r)^3}
\end{aligned}
$$

2.3.1 Case I: $\gamma = 1 \Leftrightarrow \lambda(R) = R$

Analysing the roots of the first partial derivative in order to parameter R, we get a quadratic polynomial for which we can calculate obtain the expression of the zeros, obtaining

$$
R = -\sqrt{F^*(X)r} - r \ \vee \ R = \sqrt{F^*(X)r} - r
$$

The first solution is not admissible, since it's not possible to have negative investment. Thus, we only have to check if $R = \sqrt{F(x)r} - r$ corresponds to a minimum or a maximum. To do that, we analyse the second partial derivative as stated above.

$$
\frac{\partial^2}{\partial R^2}\left(\frac{R}{R+r} F(x) - R\right) = -\frac{2rF^*(x)}{(R+r)^3} < 0
$$

where we used the fact that $R, \ r, \ F(x) > 0$.

We get then that, in order to have

$$
\arg\max_R V(x) = \sqrt{F^*(x)r} - r
$$

we need to verify

$$
F(x) > r \tag{2.1}
$$

2.3.2 Case II: $\gamma \in (0,1)$

Since the second derivative is negative for considered values of γ and $r, R > 0$, any positive root of the first partial derivative in order to R accomplishes our goal of maximizing the expression above.

When analyzing the roots of the first derivative we obtain the following polynomial,

$$R^{\gamma-1}F^*(x)r - R^{2\gamma} - 2rR^{\gamma} - r^2 = 0,$$

which unfortunately, we are not able to solve analytically for every value $\gamma \in (0,1)$. We considered some numerical illustrations for values $\gamma \in (0,1)$ presented in Section 2.4.2.

2.4 Comparative Statics

2.4.1 Benchmark and Capacity Optimization Model

efeitos de $\mu,\ \sigma,\ \delta$. In this section we study the behaviour of the decision threshold x_B^* and x_C^* and K^* as described in (**??**), with the different parameters.

Comparisons between the benchmark and capacity optimization models will be made.

Proposition: Decision thresholds x_B^* and x_C^* increase with $\sigma,\ \delta$, decrease with θ and do not have a monotonic behaviour with μ.

Proof: First note that x_B^* increases with K and it verifies $\lim_{K\to 0} x_B^*(K) = x_C^*$, $\lim_{K\to\theta/\alpha} x_B^*(K) = \infty$ and that $\forall K \in [0,\theta/\alpha) : x_B^*(K) \geq x_C^*$, where θ/α is considered to be the maximum value that the capacity can take due to restriction MENCIONAR. Thus x_C^* is a particular case of x_B^*. Since the capacity does not depend on the other parameters, we have that results that hold for x_B^*, will also hold for x_C^*.

Regarding σ, we observe that

$$\frac{\partial x_B^*(\sigma)}{\partial \sigma} = \frac{16\delta(r-\mu)\left(2\mu^2 - \mu\sigma^2\left(\sqrt{\frac{4\mu^2}{\sigma^4} - \frac{4\mu}{\sigma^2} + \frac{8r}{\sigma^2} + 1} + 1\right) + 2r\sigma^2\right)}{\sigma(\theta-\alpha K)\sqrt{\frac{4\mu^2}{\sigma^4} - \frac{4\mu}{\sigma^2} + \frac{8r}{\sigma^2} + 1}\left(\sigma^2\left(\sqrt{\frac{4\mu^2}{\sigma^4} - \frac{4\mu}{\sigma^2} + \frac{8r}{\sigma^2} + 1} - 1\right) - 2\mu\right)^2} > 0$$

The numerator is positive since, using the fact that $r > 0 \Rightarrow 2r > r$, and $r - \mu > 0$, it follows that

$$2\mu^2 - \mu\sigma^2\left(\sqrt{\frac{4\mu^2}{\sigma^4} - \frac{4\mu}{\sigma^2} + \frac{8r}{\sigma^2} + 1} + 1\right) + 2r\sigma^2 \geq 2\mu^2 - \mu\sigma^2 + 2r\sigma^2 = 2\mu^2 + \sigma^2(2r-\mu) > 2\mu^2 + \sigma^2(r-\mu) > 0. \tag{2.2}$$

On the other side, the denominator is positive (and real) since all its expressions are positive. In particular $\sqrt{\frac{4\mu^2}{\sigma^4} - \frac{4\mu}{\sigma^2} + \frac{8r}{\sigma^2} + 1} > 0$. This can be showed using the fact that $d_1 = \frac{1}{2} - \frac{\mu}{\sigma^2} + \sqrt{\left(\frac{1}{2} - \frac{\mu}{\sigma^2}\right)^2 + \frac{2r}{\sigma^2}} > 1$. Manipulating the expression we obtain that

$$d_1 - \frac{1}{2} + \frac{\mu}{\sigma^2} = \sqrt{\frac{\mu^2}{\sigma^4} - \frac{\mu}{\sigma^2} + \frac{2r}{\sigma^2} + \frac{1}{4}} > 0, \tag{2.3}$$

since $d_1 - \frac{1}{2} > \frac{1}{2} \Rightarrow d_1 - \frac{1}{2} + \frac{\mu}{\sigma^2} > 0$, for values of μ and σ such that $\mu > \left(\frac{1}{2} - d_1\right)\sigma^2$. Thus, by multiplying

the square root in (2.3) by 4, we obtain $\sqrt{\frac{4\mu^2}{\sigma^4} - \frac{4\mu}{\sigma^2} + \frac{8r}{\sigma^2} + 1}$, from which our result holds.

Regarding δ, since d_1 doesn't depend on δ, it follows that

$$\frac{\partial x_B^*(\delta)}{\partial \delta} = \frac{d_1}{d_1 - 1} \frac{\delta(r-\mu)}{\theta - \alpha K} > 0,$$

Regarding θ, we observe that if its value increases, the denominator of x_B^* increases leading x_B^* to decrease.

Regarding μ, we obtain that

$$\frac{\partial x_B^*(\mu)}{\partial \mu} = \frac{\sqrt{\sigma^4 + 4\mu^2 - 4\mu\sigma^2 + 8r\sigma^2}(\sigma^2 - 2\mu)\delta}{(\sigma^4 + 4\mu^2 - 4\mu\sigma^2 + 8r\sigma^2)(\theta - \alpha K)} = \begin{cases} < 0 & \text{for } \mu < \frac{\sigma^2}{2} \\ > 0 & \text{for } \mu > \frac{\sigma^2}{2} \end{cases}.$$

From (2.3), and in a similar way as previously done, we obtain that

$$2\sigma^2 \sqrt{\frac{\mu^2}{\sigma^4} - \frac{\mu}{\sigma^2} + \frac{2r}{\sigma^2} + \frac{1}{4}} = \sqrt{\sigma^4 + 4\mu^2 - 4\mu\sigma^2 + 8r\sigma^2} > 0$$

and that $\sigma^4 + 4\mu^2 - 4\mu\sigma^2 + 8r\sigma^2 > 0$. Then we have that, holding condition CONDICAO, the denominator is positive. Since $\delta > 0$, the non-monotone behaviour, represented above, comes for the region where $\sigma^2 - 2\mu$ is negative and positive, respectively. Note that we obtain that $\mu = \frac{\sigma^2}{2}$ is a stationary point, where the minimum value of x_B^* is observed.

□

To illustrate results above mentioned we performed some numerical illustrations, using software *Mathematica* and its function `Manipulate`. However here are only able to present static plots - we leave to the interested ones, to see the results achieved with `Manipulate`.

Unless it is written the opposite, following values were considered:

- $\mu = 0.03$
- $\sigma = 0.005$
- $r = 0.05$
- $\delta = 2$
- $\alpha = 0.01$
- $\theta = 10$
- $K = 100$

We start by illustrating how does x_B^* and x_C^* are related by the capacity level K, on which x_B^* is dependent. One can see on Figure 2.1 that conclusions mentioned on the proof (including that $x_B^*(0) = x_C^*$) hold.

On Figure 2.2 we observe that either for negative or positive values of the GBM's drift, both thresholds increase with volatility. This in accordance with [8] and [9] (VER CADERNO), whose works describe that with uncertainty is high, there is a delay time to invest, which is here reflected on an higher demand level.

Regarding the drift parameter μ we obtained that the threshold values do not have a monotonic behaviour, either for smaller or bigger values of volatility. As showed in Figure 2.3, the smallest value of demand level necessary to invest is observed at the stationary point when $\mu = \sigma^2/2$.

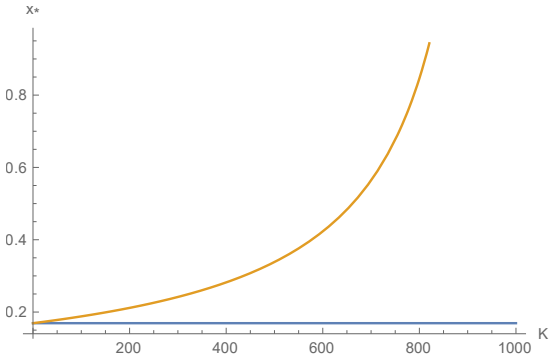

Figure 2.1: Threshold value with respect to the benchmark model (orange) and the capacity optimized model (blue), considering capacity levels $K \in [0, \theta/\alpha)$.

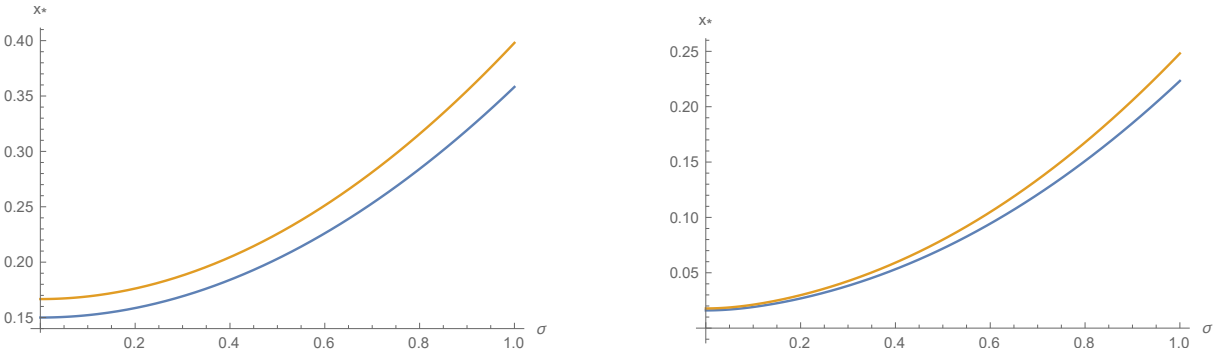

(a) $\mu = -0.7$ (b) $\mu = 0.03$

Figure 2.2: Threshold value with respect to the benchmark model (orange) and the capacity optimized model (blue), considering volatility $\sigma \in [0.0001, 1]$.

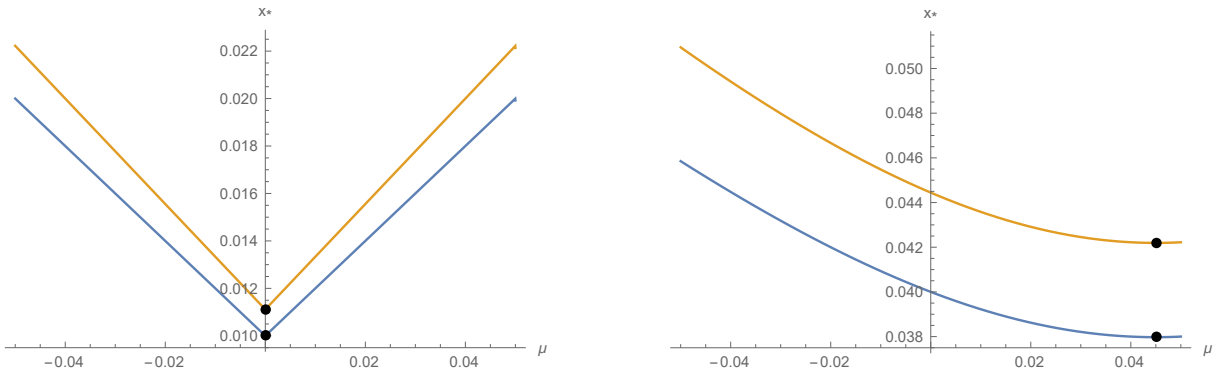

(a) $\sigma = 0.0001$ (b) $\sigma = 0.3$

Figure 2.3: Threshold value with respect to the benchmark model (orange) and the capacity optimized model (blue), considering drift $\mu \in [-r, r]$ and corresponding stationary point $\sigma^2/2$ (black).

On Figure 2.4 we observe the behaviour of both threshold levels regarding the two other parameters, sensibility level δ and innovation level θ. We have that the threshold levels increase with δ and decrease with θ.

Now we analyse optimal capacity level K_C^*, that is given by evaluating K^* as defined in (**??**) on

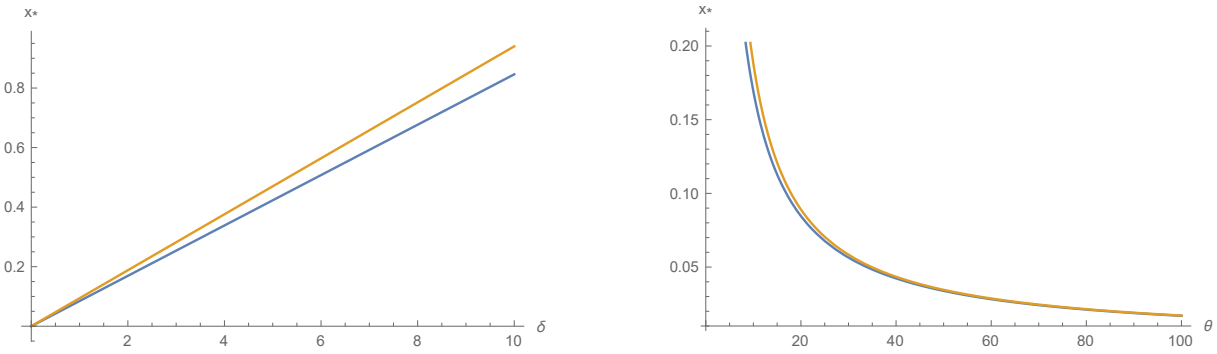

(a) $\delta \in (0, 10)$ (b) $\theta \in (\alpha K = 1, 50)$

Figure 2.4: Threshold value with respect to the benchmark model (orange) and the capacity optimized model (blue), regarding sensibility parameter δ and innovation level θ.

demand level x_C^*, as done in [10]. Its expression is given by

$$K_C^* = \frac{2\sigma^2\theta}{\alpha\left(\sigma^2\left(\sqrt{\frac{4\mu^2}{\sigma^4} - \frac{4\mu}{\sigma^2} + \frac{8r}{\sigma^2} + 1} + 3\right) - 2\mu\right)}.$$

Proposition:

Optimal capacity level K_C^* increases with μ and σ and decreases with r and α.

Proof:

The relation between K_C^* and r or α comes immediately by observing K_C^* expression.

Now, regarding drift parameter we obtain that

$$\frac{\partial K_C^*(\mu)}{\partial \mu} = \frac{4\theta\left(\sigma^2\left(\sqrt{\frac{4\mu^2}{\sigma^4} - \frac{4\mu}{\sigma^2} + \frac{8r}{\sigma^2} + 1} + 1\right) - 2\mu\right)}{\alpha\sqrt{\frac{4\mu^2}{\sigma^4} - \frac{4\mu}{\sigma^2} + \frac{8r}{\sigma^2} + 1}\left(\sigma^2\left(\sqrt{\frac{4\mu^2}{\sigma^4} - \frac{4\mu}{\sigma^2} + \frac{8r}{\sigma^2} + 1} + 3\right) - 2\mu\right)^2} > 0.$$

Since from

$$\sigma^2\left(\sqrt{\frac{4\mu^2}{\sigma^4} - \frac{4\mu}{\sigma^2} + \frac{8r}{\sigma^2} + 1} + 1\right) - 2\mu \geq 0 \Leftrightarrow \frac{4\mu^2}{\sigma^4} - \frac{4\mu}{\sigma^2} + \frac{8r}{\sigma^2} + 1 \geq \left(\frac{2\mu}{\sigma^4} - 1\right)^2 = \frac{4\mu^2}{\sigma^4} - \frac{4\mu}{\sigma^2} + 1 \quad (2.4)$$
$$\Leftrightarrow \frac{8r}{\sigma^2} \geq 0,$$

which is true for $\forall r \geq 0$, and from (2.3) we obtain that both denominator and numerator are positive, from which the result comes.

Regarding volatility parameter we obtain that

$$\frac{\partial K_C^*(\sigma)}{\partial \sigma} = \frac{8\theta\left(2\mu^2 - \mu\sigma^2\left(\sqrt{\frac{4\mu^2}{\sigma^4} - \frac{4\mu}{\sigma^2} + \frac{8r}{\sigma^2} + 1} + 1\right) + 2r\sigma^2\right)}{\alpha\sigma\sqrt{\frac{4\mu^2}{\sigma^4} - \frac{4\mu}{\sigma^2} + \frac{8r}{\sigma^2} + 1}\left(\sigma^2\left(\sqrt{\frac{4\mu^2}{\sigma^4} - \frac{4\mu}{\sigma^2} + \frac{8r}{\sigma^2} + 1} + 3\right) - 2\mu\right)^2} > 0$$

From (2.2) we obtain that the denominator is positive and from (2.3) and (2.4) that the denominator

is positive for $\forall r \geq 0$, from which the result holds.

□

Considering some numerical approximations, we observe, on Figure 2.5, that K_C^* increases with both drift and volatility. Note that, regarding the drift parameter, the growth is barely noticeable for negative values of μ, but then it turns to be logarithmic. FINANCIAL INTERPRETATION? This seems to be related with the fact that for small drift values, the future expected demand value is smaller that for positive drift values. Recall that the demand process evolves accordingly to a GBM and its expected value at time t is given by $E^{X_0=x_0}[X_t] = x_0 e^{\mu t}$.

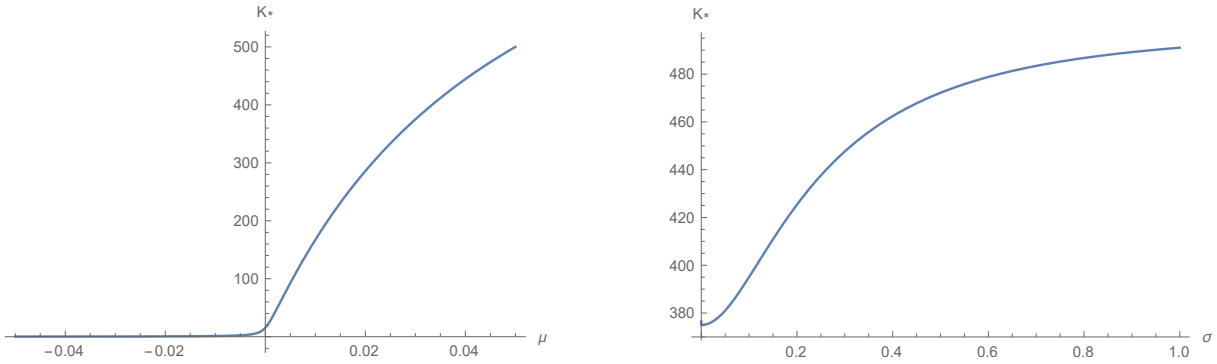

(a) $\mu \in (-r, r)$ (b) $\sigma \in (0, 1)$

Figure 2.5: Optimal capacity regarding the threshold value x_C^*.

Regarding discount rate r and sensibility parameter α, we have on Figure 2.6 that K_C^* decreases with them, as expected.

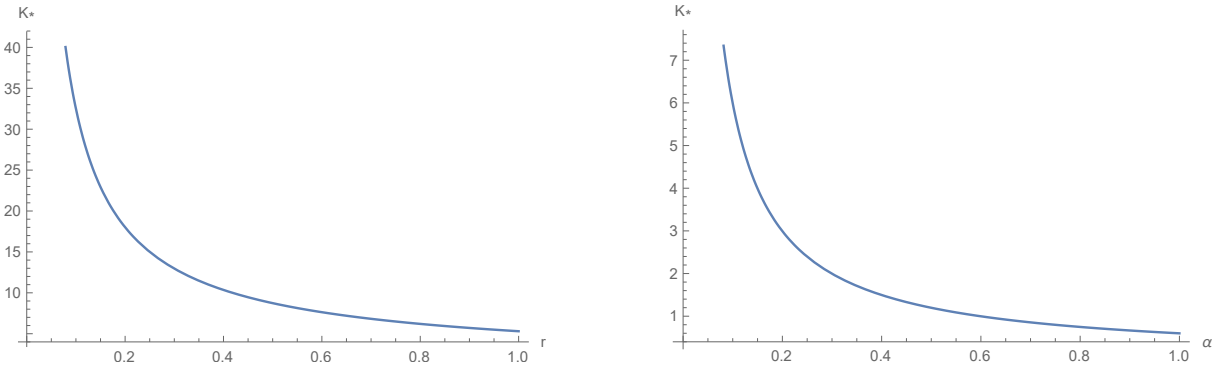

(a) $r \in (\mu, 1)$ (b) $\alpha \in (0, 1)$

Figure 2.6: Optimal capacity regarding the threshold value x_C^*.

2.4.2 R&D and Capacity Optimization Model

As stated in section 2.3, we are not able to solve analytically the polynomial presented in (**??**) for every value $\gamma \in (0, 1)$. However we considered some numerical approximations, using software *Mathematica* and its function `Solve`. For the effect, we considered

- $r = 0.05$;

- $F(X) = 10$;
- $\gamma \in (0, 1]$ incremented by 0.05.

Following results are implemented on script `RVopt.nb`.

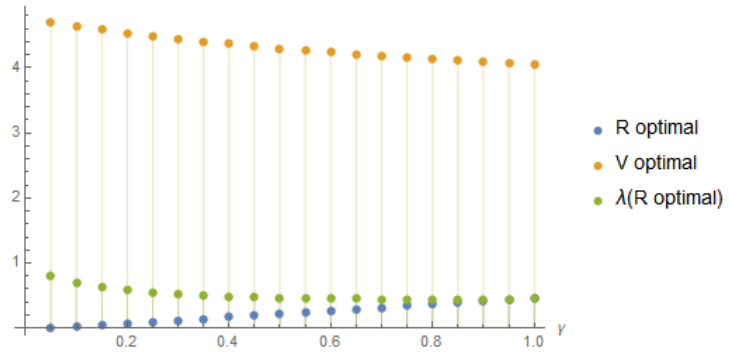

Figure 2.7: Optimal values of R and $V(X)$ for fixed values of F and r

We obtain that, although the optimal investment R grows with exponent γ, the value function for the respective optimal R decreases with exponent γ (and in a different way from the decreasing of $\lambda(R)$). We get that the smaller value of $V(X)$ is approximately 4.05, corresponding to the optimal investment level $R = 1$ and $\lambda(R) = 0.45$ and the biggest value of $V(X)$ is approximately 4.69, corresponding to the optimal investment level $R = 0.014$ and $\lambda(R) = 0.05$

The research should be supported with a comprehensive list of references. These should appear whenever necessary, in the limit, from the first to the last chapter.

A reference can be cited in any of the following ways:

- Citation mode #1 - [1]
- Citation mode #2 - Jameson et al. [1]
- Citation mode #3 - [1]
- Citation mode #4 - Jameson, Pierce, and Martinelli [1]
- Citation mode #5 - [1]
- Citation mode #6 - Jameson et al. 1
- Citation mode #7 - 1
- Citation mode #8 - Jameson et al.
- Citation mode #9 - 1998
- Citation mode #10 - [1998]

Several citations can be made simultaneously as [2, 3].

This is often the default bibliography style adopted (numbers following the citation order), according to the options:
`\usepackage{natbib}` in file `Thesis_Preamble.tex`,
`\bibliographystyle{abbrvnat}` in file `Thesis.tex`.

Notice however that this style can be changed from numerical citation order to authors' last name with the options:
`\usepackage[numbers]{natbib}` in file `Thesis_Preamble.tex`,
`\bibliographystyle{abbrvunsrtnat}` in file `Thesis.tex`.

Multiple citations are compressed when using the `sort&compress` option when loading the `natbib` package as `\usepackage[numbers,sort&compress]{natbib}` in file `Thesis_Preamble.tex`, resulting in citations like [4**?** –6].

2.5 Theoretical Model 2

Other models...

Chapter 3

ationImplement

Insert your chapter material here...

3.1 Numerical Model

Description of the numerical implementation of the models explained in Chapter 2...

3.2 Verification and Validation

Basic test cases to compare the implemented model against other numerical tools (verification) and experimental data (validation)...

Chapter 4

Results

Insert your chapter material here...

4.1 Problem Description

Description of the baseline problem...

4.2 Baseline Solution

Analysis of the baseline solution...

4.3 Enhanced Solution

Quest for the optimal solution...

4.3.1 Figures

Insert your section material and possibly a few figures...

Make sure all figures presented are referenced in the text!

Images

Figure 4.1: Caption for figure.

(a) Airbus A320

(b) Bombardier CRJ200

Figure 4.2: Some aircrafts.

Make reference to Figures 4.1 and 4.2.

By default, the supported file types are *.png,.pdf,.jpg,.mps,.jpeg,.PNG,.PDF,.JPG,.JPEG*.

See `http://mactex-wiki.tug.org/wiki/index.php/Graphics_inclusion` for adding support to other extensions.

Drawings

Insert your subsection material and for instance a few drawings...

The schematic illustrated in Fig. 4.3 can represent some sort of algorithm.

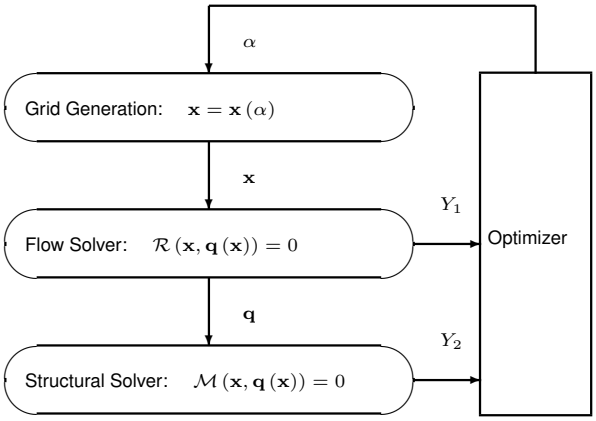

Figure 4.3: Schematic of some algorithm.

4.3.2 Equations

Equations can be inserted in different ways.

The simplest way is in a separate line like this

$$\frac{\mathrm{d}q_{ijk}}{\mathrm{d}t} + \mathcal{R}_{ijk}(\mathbf{q}) = 0\,. \tag{4.1}$$

If the equation is to be embedded in the text. One can do it like this $\partial\mathcal{R}/\partial\mathbf{q} = 0$.

It may also be split in different lines like this

$$\begin{aligned} \text{Minimize} \quad & Y(\alpha, \mathbf{q}(\alpha)) \\ \text{w.r.t.} \quad & \alpha\,, \\ \text{subject to} \quad & \mathcal{R}(\alpha, \mathbf{q}(\alpha)) = 0 \\ & C(\alpha, \mathbf{q}(\alpha)) = 0\,. \end{aligned} \tag{4.2}$$

It is also possible to use subequations. Equations 4.3a, 4.3b and 4.3c form the Naver–Stokes equations 4.3.

$$\frac{\partial \rho}{\partial t} + \frac{\partial}{\partial x_j}\left(\rho u_j\right) = 0\,, \tag{4.3a}$$

$$\frac{\partial}{\partial t}\left(\rho u_i\right) + \frac{\partial}{\partial x_j}\left(\rho u_i u_j + p\delta_{ij} - \tau_{ji}\right) = 0, \quad i = 1, 2, 3\,, \tag{4.3b}$$

$$\frac{\partial}{\partial t}\left(\rho E\right) + \frac{\partial}{\partial x_j}\left(\rho E u_j + p u_j - u_i \tau_{ij} + q_j\right) = 0\,. \tag{4.3c}$$

4.3.3 Tables

Insert your subsection material and for instance a few tables...

Make sure all tables presented are referenced in the text!

Follow some guidelines when making tables:

- Avoid vertical lines
- Avoid “boxing up” cells, usually 3 horizontal lines are enough: above, below, and after heading
- Avoid double horizontal lines
- Add enough space between rows

Model	C_L	C_D	C_{My}
Euler	0.083	0.021	-0.110
Navier–Stokes	0.078	0.023	-0.101

Table 4.1: Table caption.

Make reference to Table 4.1.

Tables 4.2 and 4.3 are examples of tables with merging columns:

An example with merging rows can be seen in Tab.4.4.

If the table has too many columns, it can be scaled to fit the text widht, as in Tab.4.5.

	Virtual memory [MB]	
	Euler	Navier–Stokes
Wing only	1,000	2,000
Aircraft	5,000	10,000
(ratio)	$5.0\times$	$5.0\times$

Table 4.2: Memory usage comparison (in MB).

	$w = 2$			$w = 4$		
	$t = 0$	$t = 1$	$t = 2$	$t = 0$	$t = 1$	$t = 2$
$dir = 1$						
c	0.07	0.16	0.29	0.36	0.71	3.18
c	-0.86	50.04	5.93	-9.07	29.09	46.21
c	14.27	-50.96	-14.27	12.22	-63.54	-381.09
$dir = 0$						
c	0.03	1.24	0.21	0.35	-0.27	2.14
c	-17.90	-37.11	8.85	-30.73	-9.59	-3.00
c	105.55	23.11	-94.73	100.24	41.27	-25.73

Table 4.3: Another table caption.

ABC	header			
	1.1	2.2	3.3	4.4
IJK	group		0.5	0.6
			0.7	1.2

Table 4.4: Yet another table caption.

Variable	a	b	c	d	e	f	g	h	i	j
Test 1	10,000	20,000	30,000	40,000	50,000	60,000	70,000	80,000	90,000	100,000
Test 2	20,000	40,000	60,000	80,000	100,000	120,000	140,000	160,000	180,000	200,000

Table 4.5: Very wide table.

4.3.4 Mixing

If necessary, a figure and a table can be put side-by-side as in Fig.4.4

Legend		
A	B	C
0	0	0
0	1	0
1	0	0
1	1	1

Figure 4.4: Figure and table side-by-side.

Chapter 5

Conclusions

Insert your chapter material here...

5.1 Achievements

The major achievements of the present work...

5.2 Future Work

A few ideas for future work...

Bibliography

[1] A. Jameson, N. A. Pierce, and L. Martinelli. Optimum aerodynamic design using the Navier–Stokes equations. In *Theoretical and Computational Fluid Dynamics*, volume 10, pages 213–237. Springer-Verlag GmbH, Jan. 1998.

[2] J. Nocedal and S. J. Wright. *Numerical optimization*. Springer, 2^{nd} edition, 2006. ISBN:978-0387303031.

[3] A. C. Marta, C. A. Mader, J. R. R. A. Martins, E. van der Weide, and J. J. Alonso. A methodology for the development of discrete adjoint solvers using automatic differentiation tools. *International Journal of Computational Fluid Dynamics*, 99(9–10):307–327, Oct. 2007. doi:10.1080/10618560701678647.

[4] A. C. Marta. A methodology for the development of discrete adjoint solvers using automatic differentiation tools. *International Journal of Computational Fluid Dynamics*, 1(9–10):307–327, Oct. 2007. doi:10.1080/10618560701678647.

[5] A. C. Marta. A methodology for the development of discrete adjoint solvers using automatic differentiation tools. *International Journal of Computational Fluid Dynamics*, 2(9–10):307–327, Oct. 2007. doi:10.1080/10618560701678647.

[6] A. C. Marta, C. A. Mader, J. R. R. A. Martins, E. van der Weide, and J. J. Alonso. A methodology for the development of discrete adjoint solvers using automatic differentiation tools. *International Journal of Computational Fluid Dynamics*, 3(9–10):307–327, Oct. 2007. doi:10.1080/10618560701678647.

[7] A. Dixit and R. S. Pindyck. *Investment Under Uncertainty*. Princeton University Press, 1^{st} edition, 1994. ISBN:978-0691034102.

[8] R. Pimentel. *Jump Processes in Finance*. PhD thesis, Instituto Superior Técnico, 2018.

[9] V. Hagspiel, K. J. M. Huisman, P. M. Kort, and C. Nunes. How to escape a declining market: Capacity investment or exit? *European Journal of Operational Research*, 254:40–50, 2016.

[10] K. J. M. Huisman and P. M. Kort. Strategic capacity investment under uncertainty. *Tilburg: Operations research*, 2013-003:40–50, 2013.

[11] R. S. Pindyck. Irreversible investment, capacity choice, and the value of the firm. *The American Economic Review*, 78:969–985, 1998.

Appendix A

Vector calculus

In case an appendix if deemed necessary, the document cannot exceed a total of 100 pages...

Some definitions and vector identities are listed in the section below.

A.1 Vector identities

$$\nabla \times (\nabla \phi) = 0 \tag{A.1}$$

$$\nabla \cdot (\nabla \times \mathbf{u}) = 0 \tag{A.2}$$

Appendix B

Technical Datasheets

It is possible to add PDF files to the document, such as technical sheets of some equipment used in the work.

B.1 Some Datasheet

SUNPOWER

C60 SOLAR CELL

MONO CRYSTALLINE SILICON

BENEFITS

Maximum Light Capture
SunPower's all-back contact cell design moves gridlines to the back of the cell, leaving the entire front surface exposed to sunlight, enabling up to 10% more sunlight capture than conventional cells.

Superior Temperature Performance
Due to lower temperature coefficients and lower normal cell operating temperatures, our cells generate more energy at higher temperatures compared to standard c-Si solar cells.

No Light-Induced Degradation
SunPower n-type solar cells don't lose 3% of their initial power once exposed to sunlight as they are not subject to light-induced degradation like conventional p-type c-Si cells.

Broad Spectral Response
SunPower cells capture more light from the blue and infrared parts of the spectrum, enabling higher performance in overcast and low-light conditions.

Broad Range Of Application
SunPower cells provide reliable performance in a broad range of applications for years to come.

The SunPower™ C60 solar cell with proprietary Maxeon™ cell technology delivers today's highest efficiency and performance.

The anti-reflective coating and the reduced voltage-temperature coefficients provide outstanding energy delivery per peak power watt. Our innovative all-back contact design moves gridlines to the back of the cell, which not only generates more power, but also presents a more attractive cell design compared to conventional cells.

SunPower's High Efficiency Advantage

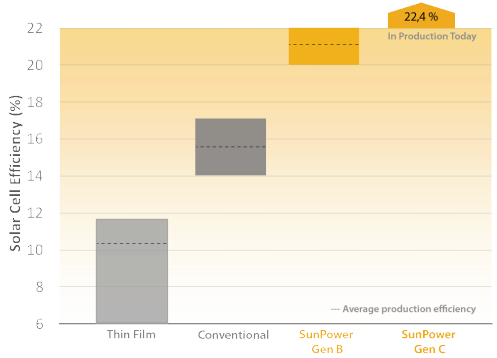

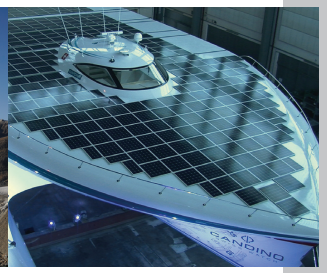

C60 SOLAR CELL

SUNPOWER

C60 SOLAR CELL

MONO CRYSTALLINE SILICON

Electrical Characteristics of Typical Cell at Standard Test Conditions (STC)

STC: 1000W/m², AM 1.5g and cell temp 25°C

Bin	Pmpp (Wp)	Eff. (%)	Vmpp (V)	Impp (A)	Voc (V)	Isc (A)
G	3.34	21.8	0.574	5.83	0.682	6.24
H	3.38	22.1	0.577	5.87	0.684	6.26
I	3.40	22.3	0.581	5.90	0.686	6.27
J	3.42	22.5	0.582	5.93	0.687	6.28

All Electrical Characteristics parameters are nominal
Unlaminated Cell Temperature Coefficients
Voltage: -1.8 mV / °C Power: -0.32% / °C

Positive Electrical Ground

Modules and systems produced using these cells must be configured as "positive ground systems".

TYPICAL I-V CURVE

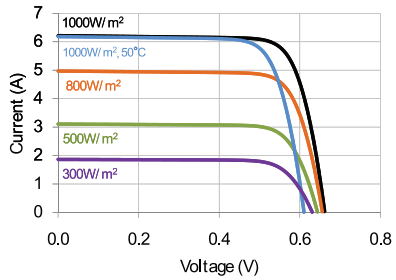

SPECTRAL RESPONSE

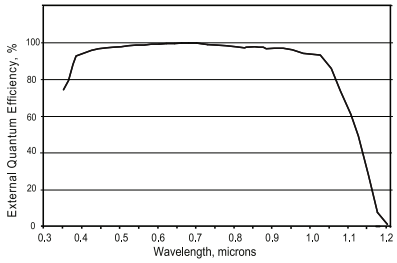

Physical Characteristics

Construction:	All back contact
Dimensions:	125mm x 125mm (nominal)
Thickness:	165µm ± 40µm
Diameter:	160mm (nominal)

Cell and Bond Pad Dimensions

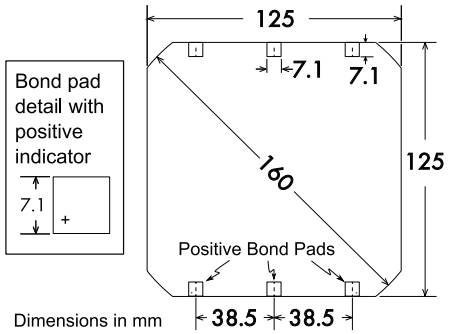

Bond pad area dimensions are 7.1mm x 7.1mm
Positive pole bond pad side has "+" indicator on leftmost and rightmost bond pads.

Interconnect Tab and Process Recommendations

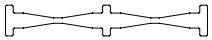

Tin plated copper interconnect. Compatible with lead free process.

Packaging

Cells are packed in boxes of 1,200 each; grouped in shrink-wrapped stacks of 150 with interleaving. Twelve boxes are packed in a water-resistant "Master Carton" containing 14,400 cells suitable for air transport.

Interconnect tabs are packaged in boxes of 1,200 each.

About SunPower

SunPower designs, manufactures, and delivers high-performance solar electric technology worldwide. Our high-efficiency solar cells generate up to 50 percent more power than conventional solar cells. Our high-performance solar panels, roof tiles, and trackers deliver significantly more energy than competing systems.

sunpowercorp.com

Document #001-66352 Rev** A4_en